Dynamics of localised states in the stochastic discrete nonlinear Schrödinger equation

Mahdieh Ebrahimi[a,*], Barbara Drossel[a], Wolfram Just[b]

[a]*Institute for Condensed Matter Physics, TU Darmstadt, Hochschulstrasse 6, Darmstadt, D-64289, Germany*
[b]*Institute of Mathematics, University of Rostock, Ulmenstraße 69, Rostock, D-18057, Germany*

Abstract

We revisit aspects of dynamics and stability of localised states in the deterministic and stochastic discrete nonlinear Schrödinger equation. By a combination of analytic and numerical techniques, we show that for deterministic motion localised initial conditions disperse if the strength of the nonlinear part drops below a threshold and that localised states are unstable in a noisy environment. As expected, the constants of motion in the nonlinear Schrödinger equation play a crucial role. An infinite temperature state emerges when multiplicative noise is applied, while additive noise yields unbounded dynamics since conservation of normalisation is violated.

Keywords: Breather, Hamiltonian dynamics, Multiplicative noise, Symplectic integration

1. Introduction

Since Holstein introduced the Discrete Nonlinear Schrödinger Equation (DNSE) model in 1950 [13] to describe polaron motion in molecular crystals, it has been widely applied to various phenomena, including wave propagation in nonlinear arrays [12], Bose-Einstein condensation in optical lattices [35, 9], and energy transport in biomolecules [32]. As a nonintegrable equation,

*Corresponding author
Email addresses: mahdieh.ebrahimi@pkm.tu-darmstadt.de (Mahdieh Ebrahimi), barbara.drossel@pkm.tu-darmstadt.de (Barbara Drossel), wolfram.just@uni-rostock.de (Wolfram Just)

the DNSE exhibits remarkable features such as chaotic trajectories, periodic orbits, and breather solutions, which are spatially localised, time-dependent excitations (see, for instance, the review [8] or the recent monograph [22]).

The DNSE is one of the few paradigmatic model systems where fundamental aspects of statistical mechanics and high-dimensional Hamiltonian dynamics have been studied in considerable detail, including non-standard features such as negative-temperature states (see e.g. the review [1]). In addition to the energy, the DNSE admits another, nontrivial, macroscopic constant of motion, which can be either identified with the normalisation condition of the state in phase space or the particle number. These two constants of motion are crucial to understand the features of the model. The statistical mechanics of such models have been coined in [26, 25, 31]. where a Gibbs measure based on the two conserved quantities, energy and particle number, has been analysed. However, this measure breaks down at negative temperatures due to the ill-defined nature of the grand canonical ensemble, and this breakdown is related to the occurrence of breather solutions [27, 28, 29, 30]. The transition to negative temperature states has much in common with first order phase transitions and the creation of thermodynamically metastable states. While the energy is predominantly contained in a few localised structures, the entropy of the system is largely determined by low-amplitude parts of the solutions. Detailed numerical studies showed that the dynamics involves extremely slow relaxation processes [14, 17]. These findings suggest that the system evolves towards a stationary state with a finite breather density and a microcanonical temperature that remains negative [21, 16, 1].

The impact of noise on the DNSE and on the spatially continuous nonlinear Schrödinger equation has been extensively studied from a rigorous mathematical point of view in considerable detail [2, 4, 3, 5, 11, 6]. While the energy, due to noise, is not any longer a constant of motion, the stochastic DNSE still preserves the particle number. Among others, the existence of a unique invariant Gibbs measure has been established for a multiplicative noise model with a phenomenological damping term [11]. Again, these studies emphasise that the conservation of normalisation is a crucial feature of the DNSE.

Here, we want to focus on the behaviour of localised solutions in a noisy environment. Since we view the DNSE as an effective equation of motion, covering for instance the evolution of a many-particle system within a mean field description, we use a formulation where we do not eliminate the pa-

rameter which measures the strength of the nonlinear part (see eq.(1)), in contrast to the standard form normally used in studies on the statistical mechanics of the model (see eq.(6)). While both descriptions are equivalent from a dynamical systems point of view, there are differences when the thermodynamic limit is considered. Our approach is more amenable to a system of finite size and may miss features which are relevant in the thermodynamic limit. Having said that, this approach enables us to map negative temperature states to positive temperature states and vice versa by changing the sign of the nonlinearity, normally called the focusing or defocusing case of the nonlinear Schrödinger equation. In section 2 we summarise some basic properties of the equations of motion and of the properties and stability of breather states, covering the focusing as well as the defocusing case. While these features are well established in the existing literature, we cover, in addition, the evolution of localised initial conditions, which tend to delocalise when the strength of the nonlinear part falls below a certain threshold value. Section 3 is devoted to the impact of noise on breather states. We will analyse two cases: multiplicative noise, which respects conservation of normalisation of the DNSE, and additive noise, which violates such a conservation law. As expected, localised states do not prevail in such noisy environments, but the former case still leads to a stationary state, emphasising the relevance of conserved quantities for the dynamics of the DNSE. Our present studies with noise correspond to an infinite temperature condition imposed on the dynamical system, so that suitable damping terms are needed to enter the more interesting finite temperature domains. Some of the implications will be addressed in the conclusion, section 4. To keep our account self-contained we also include details about the numerical integration schemes for Hamiltonian dynamics in the appendix.

2. The Discrete Nonlinear Schrödinger Equation (DNSE)

2.1. Symmetries and Transformations

We employ a version of the one-dimensional DNSE with a tunable coefficient α

$$\dot{c}_n(t) = i\Big(2c_n(t) - c_{n-1}(t) - c_{n+1}(t) - \alpha|c_n(t)|^2 c_n(t)\Big)\,. \tag{1}$$

Here, c_n represents the complex phase or amplitude at each site n, where we assume a system of size L imposing periodic boundary conditions $c_n = c_{n+L}$. The parameter α controls the strength of the nonlinearity. The choice $\alpha > 0$ leads to a so-called focusing and the choice $\alpha < 0$ to a so-called defocusing nonlinear Schrödinger equation. The equation of motion, eq. (1), constitutes a Hamiltonian system where $\{c_n, \bar{c}_n\}$ are canonical conjugate variables, and the Hamiltonian itself is given by

$$H = \sum_{n=0}^{L-1} \left(2|c_n|^2 - c_n \bar{c}_{n-1} - c_n \bar{c}_{n+1} - \frac{\alpha}{2} |c_n|^4 \right) . \tag{2}$$

Using the appropriate Poisson bracket

$$\{F, G\} = i \sum_n \left(\frac{\partial F}{\partial \bar{c}_n} \frac{\partial G}{\partial c_n} - \frac{\partial F}{\partial c_n} \frac{\partial G}{\partial \bar{c}_n} \right) , \tag{3}$$

the DNSE can be cast into the form of canonical equations of motion

$$\dot{c}_n(t) = i \frac{\partial H}{\partial \bar{c}_n} = \{H, c_n\} = i \mathbf{L} c_n \tag{4}$$

where $\mathbf{L}$ denotes the Liouville operator $i\mathbf{L}\cdot = \{H, \cdot\}$. Incidentally, eq. (3) imposes a sign convention which also determines the sign of the Hamiltonian (2).

It is a key feature of the nonlinear Schrödinger equation that it admits two conserved quantities, namely, the system's total energy $E = H$ and the normalisation of the wave function or the particle number

$$N = \sum_{n=0}^{L-1} |c_n|^2 , \tag{5}$$

as can be easily derived from $\{H, N\} = 0$. In our setup, we chose $N = 1$ and let the total energy E and the on-site potential strength α be the two independent parameters of the dynamics.

The DNSE is often used in non-dimensional units (see e.g. [27, 1]) where it takes the form

$$i\dot{C}_n = C_{n+1} + C_{n-1} + |C_n|^2 C_n . \tag{6}$$

This form is obtained from eq. (1) by performing the phase transformation $c_n \mapsto \exp(-i2t) c_n$ and applying the scaling $c_n \mapsto \sqrt{|\alpha|} c_n$ in the focusing case

$\alpha > 0$. In the defocusing case, $\alpha < 0$, this procedure results in eq. (6), with a negative sign of the cubic term. For systems with an even number of lattice sites such an equation with negative cubic term can be transformed into the normal form, eq. (6), by using $c_n \mapsto (-1)^n \bar{c}_n$. Thus, for the DNSE there is no fundamental difference between the focusing and the defocusing case from a dynamical systems point of view. The two conserved quantities of eq. (6) are the energy $\tilde{H}$ and the particle number $\tilde{N}$

$$\begin{aligned} \tilde{H} &= \sum_{n=0}^{L-1} \left(C_n \bar{C}_{n+1} + C_n \bar{C}_{n-1} + \frac{1}{2} |C_n|^4 \right), \\ \tilde{N} &= \sum_{n=0}^{L-1} |C_n|^2 \end{aligned} \tag{7}$$

which are considered to be the two parameters of the system. The dynamical behaviour of the model can be captured by phase diagrams which are presented in terms of these quantities [27, 1]. Using the above transformations between the C_n and c_n, the values of these conserved quantities can be expressed in terms of eqs. (2) and (5) as

$$\tilde{H} = \alpha(2N - H) = \alpha(2 - E), \qquad \tilde{N} = |\alpha| N = |\alpha| \,. \tag{8}$$

In the following, we present our results in terms of eq. (1) with $N = 1$ and the two parameters E and α, while eq. (8) can be used to translate those results to the non-dimensional version eq. (6). Note that due to the normalisation condition the energy E is not extensive, so that $-\alpha/2 \leq E \leq 4 - \alpha/(2L)$ if $\alpha > 0$, and $-\alpha/(2L) \leq E \leq 4 - \alpha/2$ if $\alpha < 0$.

2.2. Breathers and their Stability

The nonlinear Schrödinger equation is one of the paradigmatic model systems where time-dependent spatially localised solutions, so-called breathers, have been studied in considerable detail [20]. Here we summarise a few of the main well-known features. In the context of eq. (1) the simplest type of breather solution has the form $c_n(t) = \exp(i\Omega t) r_n$, where the frequency Ω determines the period of the breather and r_n the real-valued spatially localised shape. With eqs. (1) and (5) we obtain the nonlinear eigenvalue problem

$$0 = (2 - \Omega - \alpha r_n^2) r_n - r_{n-1} - r_{n+1}, \qquad \sum_{n=0}^{L-1} r_n^2 = 1 \tag{9}$$

which can be solved straightforwardly by numerical root-finding methods (see figure 1). Eq. (2) provides a relation between the shape of the breather and its energy, i.e., a relation between α and the energy

$$E_\alpha = \sum_{n=0}^{L-1} \left(2r_n^2 - r_n r_{n-1} - r_n r_{n+1} - \frac{\alpha}{2} r_n^4 \right) . \tag{10}$$

For large $|\alpha|$, the r_n and Ω can be determined by performing an expansion of all these quantities in powers of $1/\alpha$ and keeping the leading terms only. If the breather has its maximum at lattice site $n = c$, i.e. $r_c \geq |r_n|$, one obtains

$$\begin{aligned} r_c &= 1 - \frac{1}{\alpha^2} + \mathcal{O}(|\alpha|^{-3}) \\ r_{c\pm1} &= \frac{1}{\alpha} + \frac{1}{\alpha^3} + \mathcal{O}(|\alpha|^{-4}) \\ r_{c\pm k} &= \alpha^{-|k|} + \mathcal{O}(|\alpha|^{-(|k|+1)}) \quad \text{for} \quad k \geq 2 \\ \Omega &= -\alpha + 2 + \mathcal{O}(|\alpha|^{-2}) \\ E_\alpha &= -\frac{\alpha}{2} + 2 - \frac{2}{\alpha} + \mathcal{O}(|\alpha|^{-2}) . \end{aligned} \tag{11}$$

The DNSE admits in the focusing case, i.e., for $\alpha > 0$, a breather, which is unimodal since all r_n are positive. This solution can be mapped onto a solution for the defocusing case ($\alpha < 0$) by the transformation $r_n \to (-1)^n r_n$ (see section 2.1), giving a staggered breather with the same unimodal envelope (see figure 1).

When α is very small and positive, the breather becomes very broad, and the difference $r_n - r_{n-1}$ becomes small. In such a continuum limit the amplitudes r_n can be captured by a smooth function $\Phi(x)$ via the scaling $r_n = \Phi(n/L)/\sqrt{L}$. In such a continuum limit, we assume, for simplicity, a system of length one, in non-dimensional units. Then the normalisation condition in eq. (9) becomes the Riemann sum of the integral constraint $\int_0^1 |\Phi(x)|^2 dx = 1$ and the discrete second derivative $2r_n - r_{n-1} - r_{n+1}$ to leading order can be written as $-\Phi''(x)/L^2$ with $x = n/L$. Hence, eq. (9) becomes

$$0 = -\Phi''(x) - \Omega L^2 \Phi(x) - \alpha L |\Phi(x)|^2 \Phi(x) . \tag{12}$$

To obtain a well defined continuum limit, $L \to \infty$, we impose the scaling relations $\Omega \sim L^{-2}$ and $\alpha \sim L^{-1}$, so that the profile of the breather solution is captured by eq. (12). This limit permits a formal expansion in powers of

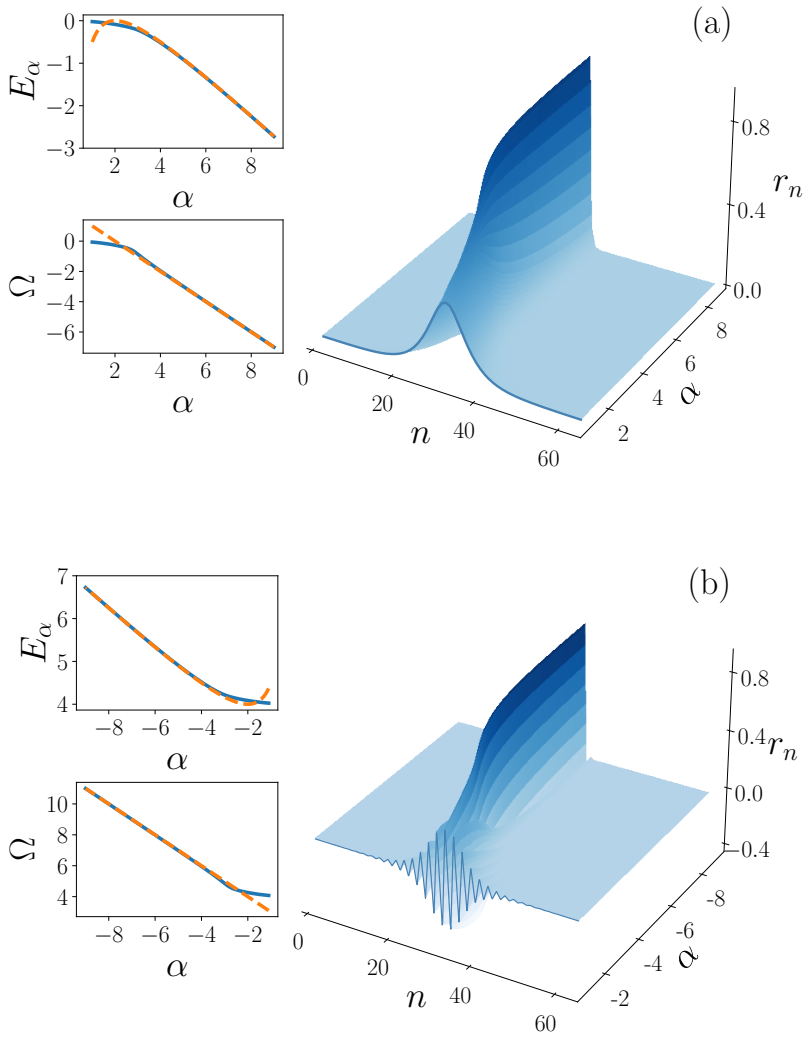

Figure 1: (a) Spatial profile r_n of a breather in dependence on α for (a) the focusing and (b) the defocusing DNSE, obtained from eq. (9) for a system of size $L = 64$. The insets show the respective dependence of the energy E and of the breather frequency Ω on α (blue, solid lines), as well as the leading order asymptotic expression in eq. (11) (amber, broken line).

α, which is complementary to eq. (11), the asymptotic of the breather for large values of α.

In contrast, for negative α such an approach cannot be used directly due to the staggered character of the breather, which means that the continuum limit for $\alpha \to 0-$ is singular.

The stability of the breather states can be determined in terms of a linear stability analysis. Using the notation $c_n(t) = \exp(i\Omega t)(r_n + \delta r_n(t) + i\delta\varphi_n(t))$ in eq. (1) and expanding to linear order in the δr_n and $\delta\varphi_n$, one obtains the eigenvalue problem

$$\begin{aligned}\Lambda \begin{pmatrix} \delta r_n \\ \delta\varphi_n \end{pmatrix} = & \begin{pmatrix} 0 & -(2-\Omega-\alpha r_n^2) \\ 2-\Omega-3\alpha r_n^2 & 0 \end{pmatrix} \begin{pmatrix} \delta r_n \\ \delta\varphi_n \end{pmatrix} \\ & + \begin{pmatrix} 0 & -1 \\ 1 & 0 \end{pmatrix} \begin{pmatrix} \delta r_{n-1} \\ \delta\varphi_{n-1} \end{pmatrix} \\ & + \begin{pmatrix} 0 & -1 \\ 1 & 0 \end{pmatrix} \begin{pmatrix} \delta r_{n+1} \\ \delta\varphi_{n+1} \end{pmatrix} . \end{aligned} \tag{13}$$

Such an equation holds for every n, which means that the eigenvalues of a $2L \times 2L$ matrix must be evaluated for stability. This matrix has blocks of size 2×2 on the diagonal and on the first off-diagonals. Because of the symplectic structure, eigenvalues come in quadruples $\pm\Lambda, \pm\bar{\Lambda}$. In our case, eigenvalues are always imaginary (see figure 2). While in general such a feature is not a sufficient condition for stability of a fixed point in Hamiltonian systems (see e.g. [24]) in our case there is consensus that such a breather corresponds to an extremum of the Hamiltonian and thus inherits stability (but not asymptotic stability) for any non-vanishing value of α. A breather solution where the maximum of the shape occurs on a bond and not at a lattice site yields eigenvalue pairs with finite real parts, and such breathers are linearly unstable. All these features are well known (see e.g. [7]), but to the best of our knowledge a formal analytic proof covering the whole range of α values has not been established so far.

The structure of the spectrum shown in Fig. 2 can be derived from eq. (13) with the usual arguments borrowed from scattering theory. First there occurs a pair of zero eigenvalue caused by the phase and the time translation invariance of the original equation of motion. This pair of Goldstone modes is related to the conservation of H and N, since conservation of H leads to time translation invariance, and conservation of N to invariance under a change of phase. The other eigenvalues are imaginary and are grouped in two quasi-continuous bands with $\mathrm{Im}(\Lambda) \in [|\Omega|, |\Omega|+4] \cup [-|\Omega|-4|, -|\Omega|$ (see the two insets in figure 2) with the corresponding eigenfunctions behaving

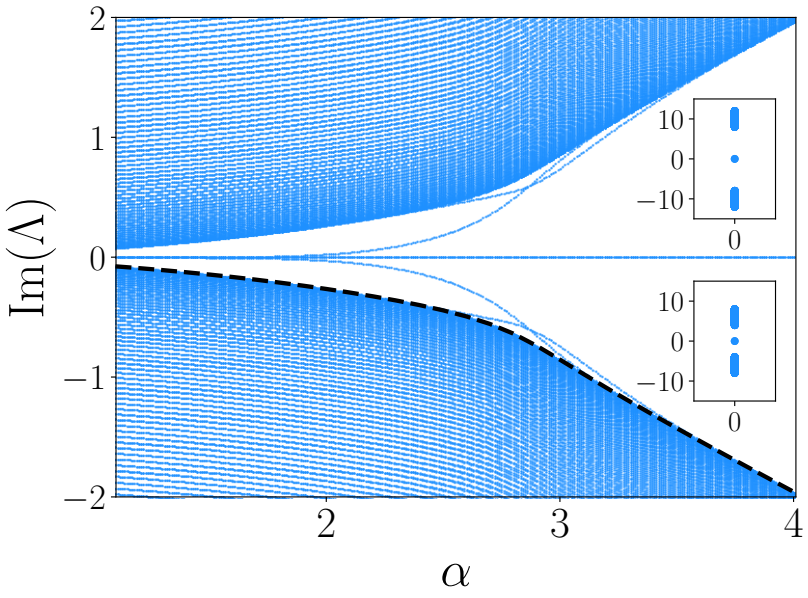

Figure 2: Eigenvalues (imaginary part) in dependence on α of the linear stability problem for unimodal breather solutions, see eq. (13), computed for a system of size $L = 256$. The real part vanishes. The broken line shows the dependence of the breather frequency Ω on α (cf. Fig. 1). The two insets show the location of eigenvalues in the complex plane for $\alpha = 10$ (upper inset) and $\alpha = 6$ (lower inset).

asymptotically like plane waves. When α decreases these two bands approach each other and two isolated eigenvalues detach from these quasi-continuous bands, with the corresponding eigenfunctions being exponentially localised. One pair of these localised eigenstates approaches zero at an exponential rate. This eigenstate is the precursor of another Goldstone mode which occurs in the continuum limit and which is related with the space translation invariance. The region shown in detail in figure 2 shows a qualitative transition for α values at about 3. For large values of α the frequency Ω and the eigenvalues are to leading order linear functions of α with slope 1, see eq.(13). This behaviour corresponds to the so-called anti-integrable limit of the DNSE. This feature persists down to α values at around three, where a substantial curvature becomes noticeable and an expansion based on the anti-integrable limit may break down. The behaviour of the spectrum for smaller values of α seems to be dominated by the continuum limit $\alpha \to 0$, and the transition between these two regimes seems to be surprisingly sharp.

2.3. Localised initial condition and time evolution

If the DNSE is viewed as an effective equation of motion for a many-particle wave function, a state $c_n(0) = \delta_{n,c}$ that is fully localised at a lattice site $n = c$ is a natural initial condition. Such an initial state is close to a breather state, at least for larger α, and the question arises whether the wave function remains localised under time evolution.

Computation of solutions of eq. (1) by numerical means requires some care. Bog standard numerical integration schemes for ordinary differential equations normally do not preserve energy and thus induce uncontrollable drifts which render the long time results meaningless. Hence symplectic integrators are needed to deal with Hamiltonian dynamics [10], so that the energy is preserved at least approximately, which means that energy fluctuations stay bounded in time. Unless Hamiltonians have a very peculiar structure such symplectic schemes may result in implicit integration schemes, and there is no a priori guarantee that they preserve any other constant of motion, such as the particle number N. Following for instance the basic exposition of [33] which was inspired by previous work [36] on leapfrog integration methods, we use here an explicit symplectic integration scheme which by design will also preserve N. The main idea is to factorise the time evolution operator $\exp(i\mathbf{L}\Delta t)$ by decomposing $\mathbf{L}$ into the linear nearest-neighbour coupling term and the nonlinear onsite term, both of which are integrable (see appendix Appendix A.1 for more details).

Using an initial condition $c_n(0) = \delta_{n,c}$ we compute time traces of the energy $E(t)$, the normalisation $N(t)$, and the largest probability $p_{max}(t) = \max\{|c_n(t)|^2 : 1 \leq n \leq L\}$ for different values of α (see figure 3). By design, the values of energy and normalisation are preserved, and the small numerical fluctuations give a rough impression of the numerical accuracy (see figure 3(b) and 3(c)). The maximal probability $p_{max}(t)$ is a simple proxy for the degree of localisation of the state $\{c_n(t)\}$. If that value is close to 1, the state is almost δ localised. Smaller time-dependent values that oscillate but do not decay still indicate some degree of localisation. Decay towards very small values of $p_{max}(t)$ indicates that localisation is lost and the wave function becomes delocalised.

For large values of α, the energy of the initial condition $E_{init} = 2-\alpha/2$ (see eq. (2)) is almost identical to the energy of the breather state (see eq. (11)) and the resulting time-dependent state performs small oscillations in the vicinity of the stable breather solution. With decreasing α, the distance of the initial condition from the breather state increases so that the extent of

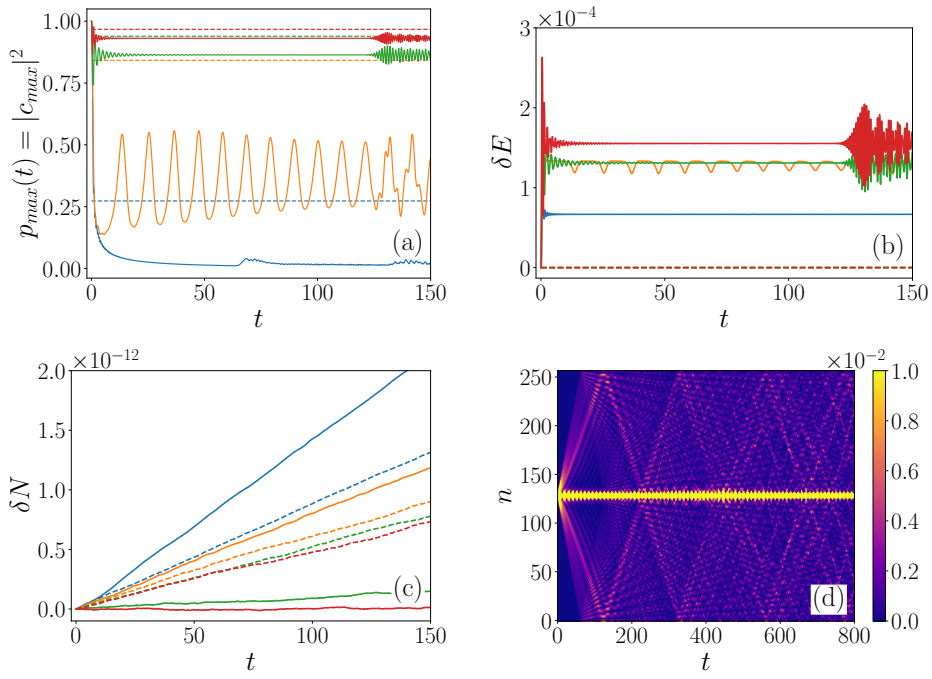

Figure 3: Time evolution of eq. (1) for system size $L = 256$ and with δ-peak initial condition $c_n(0) = \delta_{n,128}$. The numerical integration was done using a symplectic integration scheme (see appendix Appendix A.1 for details) with stepsize $\tau = 0.01$. (a) Time traces of the amplitude $p_{max}(t)$ (the maximum of $|c_n(t)|^2$) for different values of α: $\alpha = 2$ (blue line), $\alpha = 4$ (orange line), $\alpha = 6$ (green line), and $\alpha = 8$ (red line). The dotted horizontal line shows the maximal probability of the corresponding stable breather state. (b) Time evolution of the deviation of the energy from the initial energy $\delta E(t) = E(t) - E_{init}$ and (c) the deviation of the normalisation $\delta N(t) = N(t) - 1$ for the same set of α values as in part (a). Full lines show the data when the δ-peak initial condition has been used, broken lines show the data when the corresponding breather state has been used as initial condition. (d) Spatio temporal density plot for the evolution of $|c_n(t)|^2$ for $\alpha = 4$ with emission of plane waves from the central peak and recurrence due to periodic boundary conditions, The peak exceeds 0.1, but we chose this colour scheme to highlight the recurring fluctuations in greater detail. (see as well panel (a) and (b)).

localisation decreases, and the oscillations of the time-dependent solutions become more pronounced (see figure 3(a)). The localised state breaks down at about $\alpha \approx 3.5$ for $L = 1024$. Such a breakdown is, however, not a signature of any dynamical instability. The particular initial condition is not any longer contained in the region of the phase space which constitutes the elliptic island of the stable breather solution (see as well, for instance, [22] p.321). The time-

dependent dynamics of the localised solution is accompanied by a recurrence phenomenon whereby the localised part of the solution emits plane waves which recur after finite time, due to periodic boundary conditions (see figure 3(d)), causing an approach towards a stationary state where a localised peak oscillates in a chaotic fashion.

3. The Stochastic Discrete Nonlinear Schrödinger Equation (SDNSE)

We want to study the stability of the breathers with respect to white noise. We will here address two choices of stochastic perturbations, a multiplicative noise that preserves the normalisation, and a simple generic additive noise. To keep mathematical formalities at a minimum we will consider noise in the sense of Stratonovich. In physics terms that means the noise is supposed to have a very small but finite correlation time, which can be disregarded at the time scales of interest. In particular, one does not need to employ any sophisticated stochastic calculus and can treat the noise merely as an ordinary function when computing solutions of a stochastic differential equation. For this reason, we can again apply the symplectic integration scheme by extending it to non-autonomous systems and pooling the noise term together with the nonlinear term when factorising the time evolution operator (see appendix Appendix A.2).

3.1. Multiplicative Noise Model

When a multiplicative noise term is included, the equation of motion (1) becomes

$$\begin{aligned}\dot{c}_n(t) =& i\left(2c_n(t) - c_{n-1}(t) - c_{n+1}(t) - \alpha|c_n(t)|^2 c_n(t)\right) \\ &+ i\sigma c_n(t)\xi_n(t)\,.\end{aligned} \tag{14}$$

Here $\xi_n(t) \in \mathbb{R}$ denotes real-valued uncorrelated Gaussian random white noise with correlation function

$$\langle \xi_n(t)\xi_m(s)\rangle = \delta_{n,m}\delta(t-s)\,, \tag{15}$$

and the parameter $\sigma \in \mathbb{R}$ determines the strength of the noise. Eq. (14)) constitutes still a Hamiltonian system with time-dependent stochastic Hamil-

tonian

$$\begin{aligned} H_\sigma(t) &= \sum_{n=0}^{L-1} \Big(2|c_n|^2 - c_n\bar{c}_{n-1} - c_n\bar{c}_{n+1} - \frac{\alpha}{2}|c_n|^4 \\ &\quad +\sigma|c_n|^2\xi_n(t) \Big) \\ &= H + \sigma \sum_{n=0}^{L-1} |c_n|^2 \xi_n(t) \end{aligned} \tag{16}$$

as can be easily confirmed using eq. (4). Since $\{H_\sigma(t), N\} = 0$ we obtain conservation of the normalisation even in this stochastic case so that a multiplicative Stratonovich noise does not affect the normalisation.

To study the robustness of the breather solution against multiplicative noise, we perform numerical simulations of the stochastic differential equation (14) for various parameter values, where we take the particular breather as an initial condition. In the literature, one can find sophisticated numerical integration schemes for symplectic stochastic systems (see e.g. [10] for a comprehensive review) which are implicit and thus more difficult to implement, and there is a priori no guarantee that such schemes preserve a constant of motion. In contrast, our explicit higher-order integration scheme (see appendix Appendix A.2) observes the conservation of N by design and is straightforward to apply. The resulting time traces for the energy and the maximal probability are shown in figure 4 for a range of noise amplitudes σ and α values that support a localised breather state. The energy seems to depend on the effective time variable $\sigma^2 t$ only, in line with simple diffusion processes. The energy increases initially linearly, with a slope roughly proportional to α^{-1}, and then saturates with fluctuations around $E \approx 2$. The maximal probability decays as well on a joint time scale $\sigma^2 t$. The localised state is destroyed by the noise in favour of a delocalised state, which spreads across the system.

We can obtain a better quantitative analysis by looking at mean values averaged over an ensemble of orbits. In all cases we take again the corresponding breather state as initial condition. For the time dependence of the energy we observe an almost perfect data collapse when a rescaled time variable $\sigma^2 t/\alpha$ is employed, see figure 5(a). The mean energy shows initially a linear increase with constant slope, where the observed offset for different values of α is simply caused by the dependence of the initial energy on α. The finding that the initial slope of $\dot{E}$ is proportional to $1/\alpha$ can be explained

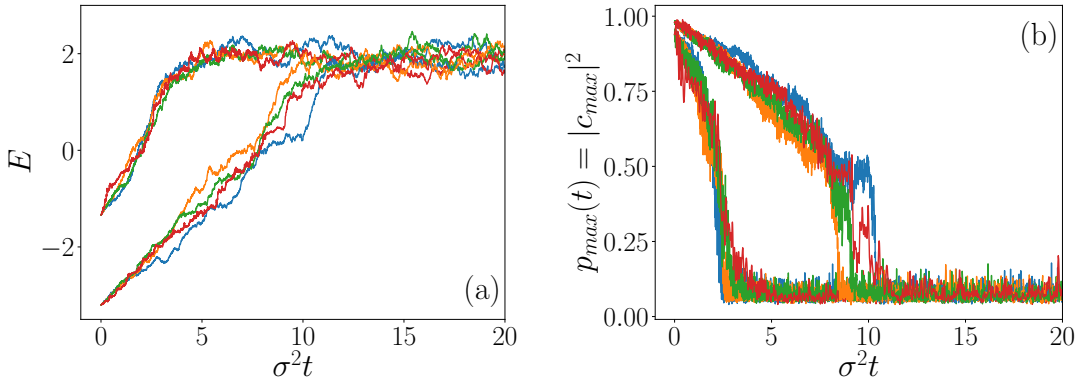

Figure 4: Time traces obtained from numerical simulations of the multiplicative noise model eq. (14)) for system size $L = 64$ and different noise levels: $\sigma = 0.01$ (blue), $\sigma = 0.03$ (orange), $\sigma = 0.3$ (green), and $\sigma = 0.1$ (red). Data are shown on a rescaled time scale $\sigma^2 t$. (a) Time dependence of the energy, eq. (2), for $\alpha = 6$ (upper set of curves) and $\alpha = 10$ (lower set of curves). (b) Time dependence of the largest probability $p_{max}(t)$ for $\alpha = 6$ (lower set of curves) and $\alpha = 10$ (upper set of curves). For all α the corresponding deterministic breather state was chosen as initial condition (cf. eq. (11)).

to some extent by considering the parameter-free version eqs. (6-8) of the model: If the shape of the decaying breather is essentially determined by its energy $\tilde{H}$, the time evolution of $\tilde{H}$ depends mainly on $\tilde{H}$ itself, irrespective of the value of α. Using the relation $E \propto \tilde{H}/\alpha$, we find $\dot{E} \propto 1/\alpha$.

The time evolution of the amplitude of the state, $p_{max} = \max\{|c_k|^2\}$ shows a different characteristic, see figure 5(b). As already reported in [18] there occur two different temporal regimes. For smaller times, roughly speaking as long as $p_{max}(t) > 1/2$, we obtain a quite accurate data collapse with respect to the noise amplitude, so that the amplitude is effectively a function of $\sigma^2 t$. For larger times, say $p_{max}(t) < 1/2$, that scaling deteriorates and a mild additional dependence on the noise amplitude becomes visible. Overall the distinction between these two temporal regimes becomes more pronounced if the on-site potential strength α increases. Furthermore, the overall dependence of p_{max} on α differs from the scaling properties of the energy. To highlight this point further it is sensible to look a the lifetime of the breather state. There is no unique way to assign such a lifetime. We adopt here the definition of a (stochastic) lifetime such that the value of $p_{max}(t)$ drops for the first time below half of its initial value. The mean of this lifetime, τ_{BLT}, in dependence on α is shown in figure 5(c). We still observe

the aforementioned scaling of the lifetime with σ^2. The dependence of τ_{BLF} on α shows also a quadratic behaviour for larger values of α (see as well the inset in figure 5(c)). As a consequence, we observe a reasonable data collapse for larger values of α when p_{max} is considered in dependence of the rescaled time variable $\sigma^2 t/\alpha^2$, see figure 5(d). In particular, this behaviour shows that other definitions of a mean lifetime would give quantitatively analogous results. In summary, mean values seem to depend on the rescaled time $\sigma^2 t$ in the range of noise amplitudes employed here, while the dependence on the on-site potential strength α is more subtle and depends on the quantity under consideration. That the decay time of p_{max} is for large α proportional to α^2 can be made plausible by considering eqs. (1) and (11): the time evolution of p_{max} has a nonlinear term proportional to α, which tends to preserve the maximum value, and the term that transfers weight to the two neighbors is proportional to $r_{c\pm1}$, which in turn is proportional to $1/\alpha$. This is weaker by a factor $1/\alpha^2$ compared to the main term that counteracts destruction of the breather.

The time traces suggest that the stochastic dynamics tends towards a stationary state that is characterised by a finite value of energy $E \approx 2$, irrespective of the value of α and of the initial condition. Indeed, it is plausible to assume that the system is ergodic: the noise term gives the c_n random kicks that change their phases, and the nearest-neighbour coupling subsequently changes the amplitudes, while keeping the overall normalisation at one, so that the energy cannot escape to infinity. In this way, the noise can push the state of the system through phase space, as there is no restoring force that tends back to the initial state. Eventually, the boundary of the region of linear stability of the breather will be passed, and the long-term behaviour will be dominated by the maximum entropy distribution of the c_n. Ergodicity implies a long-term behaviour that results in a uniform distribution of the c_n on the surface of the $2L$-dimensional unit sphere

$$\rho_{mc}(\{c_n, \bar{c}_n\}) = \frac{1}{Z_{mc}} \delta\left(N - 1\right) \tag{17}$$

with

$$\begin{aligned} Z_{mc} &= \int_{\mathbb{C}^L} d(c_1, \bar{c}_1, c_2, \bar{c}_2, \ldots, c_L \bar{c}_L) \delta\left(N - 1\right) \\ &= \frac{\pi^L}{(L-1)!} \end{aligned} \tag{18}$$

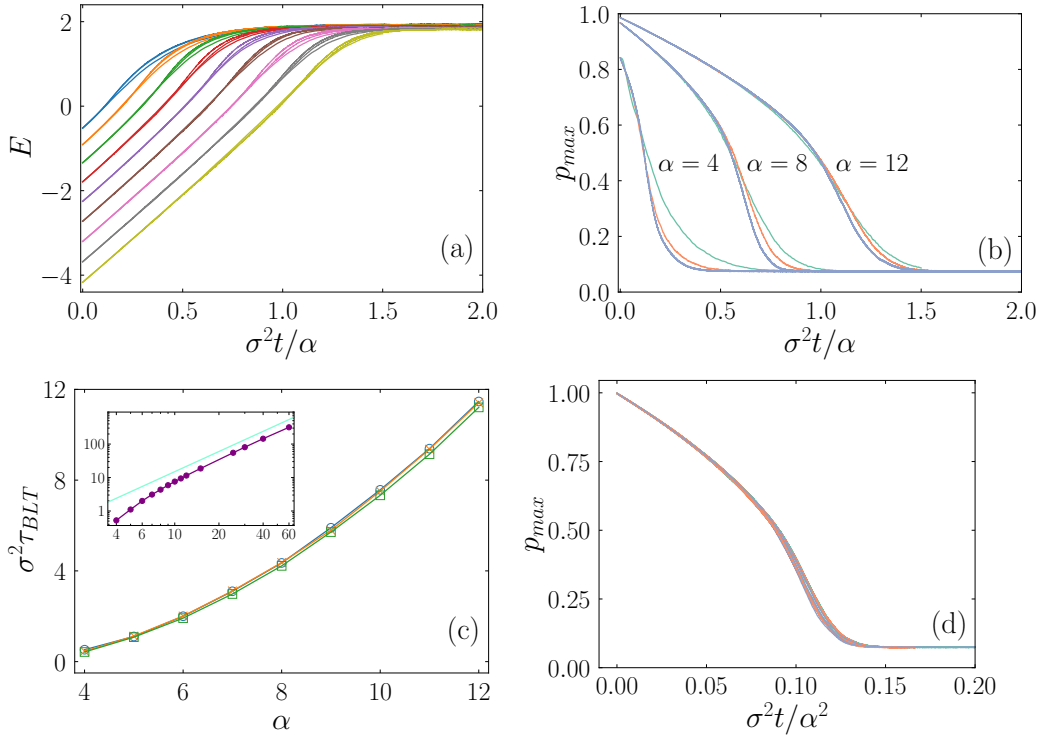

Figure 5: Ensemble averages of time traces of the SDNSE, eq. (14), with system size $L = 64$ and with breather state as initial condition (cf. eq. (11)). Means have been computed over 10^3 realisations of the noise. (a) Mean energy E as a function of a rescaled time, $\sigma^2 t/\alpha$, for different values of α (from left to right: $\alpha = 4$, 5, 6, ..., 11, 12) and three values of the noise amplitude, $\sigma = 0.3$, 0.1 and 0.03. For given value of α the three curves for different noise amplitude almost overlap at the scale of the graph. (b) Amplitude p_{max} of the spatial pattern as a function of the rescaled time, $\sigma^2 t/\alpha$, for different α and σ values (green: $\sigma = 0.03$, orange: $\sigma = 0.1$, blue: $\sigma = 0.3$). (c) Mean lifetime of the breather, τ_{BLT}, in dependence of α for three different values of the noise amplitude (square: $\sigma = 0.03$, circle: $\sigma = 0.3$, cross: $\sigma = 0.1$, the lines are a guide to the eye). The inset shows the mean lifetime on a double logarithmic scale (for $\sigma = 0.3$). The straight line in the inset has slope 2. (d) p_{max} in dependence on the rescaled time variable $\sigma^2 t/\alpha^2$ for $\alpha = 25$, 30, 40 and $\sigma = 0.3$, 0.1, 0.03. All twelve curves overlap at the scale of the graph.

With a slight abuse of the standard notation (see e.g. [34]) we call eq. (17) simply a "microcanonical" distribution, since N is the conserved quantity in the stochastic setup.

Our ergodic system of L variables c_n satisfies the constraint $\sum_n (\mathrm{Re}(c_n)^2 + \mathrm{Im}(c_n)^2) = N$, a condition which is formally equivalent to a system of L

independent harmonic oscillators for which the total energy $H = \sum_n (p_n^2 + q_n^2)$ is conserved. In this setup the equivalence of ensembles in the thermodynamic limit can be shown by elementary methods. The equivalent of a canonical ensemble for the harmonic oscillators (where the mean energy is determined by the temperature) is a grand canonical ensemble of our system, where a chemical potential ν determines the average particle number $\langle N \rangle$. Hence for large system size L the "microcanonical" ensemble, eq. (17)) is equivalent to the grand canonical ensemble

$$\rho_{gc}(\{c_n, \bar{c}_n\}) = \frac{1}{Z_{gc}} \exp\left(-\nu N\right) \tag{19}$$

with

$$Z_{gc} = \frac{\pi^L}{\nu^L}. \tag{20}$$

The chemical potential ν is calculated via

$$\langle N \rangle_{gc} = -\frac{\partial}{\partial \nu} \ln Z_{gc} = \frac{L}{\nu} = 1\,, \tag{21}$$

giving $\nu = L$. Since the distribution eq. (19) does not involve the Hamiltonian H, it corresponds formally to a situation of infinite temperature, which is also evident from the fact that the different c_n are uncoupled in eqs. (17) and (19).

For comparison of these analytical predictions with the simulation data we resort to the marginal distributions, e.g., to the distribution of a single amplitude c_1. The microcanonical and the grand canonical distribution yield

$$\begin{aligned} p_{mc}(c_1, \bar{c}_1) &= \int_{\mathbb{C}^{L-1}} d(c_2, \bar{c}_2, c_3, \bar{c}_3, \ldots, c_L \bar{c}_L) \rho_{mc}(\{c_k, \bar{c}_k\}) \\ &= \frac{L-1}{\pi} \left(1 - |c_1|^2\right)^{L-2}, \quad (|c_1|^2 \leq 1) \end{aligned} \tag{22}$$

and

$$p_{gc}(c_1, \bar{c}_1) = \frac{L}{\pi} \exp\left(-L|c_1|^2\right) \tag{23}$$

respectively. Both expressions, eqs. (22) and (23), virtually do not differ for moderate or large system size, and both coincide with the numerical data obtained in the stationary state (see figure 6(a)). However, small finite size corrections are discernible in the data close to zero (inset in figure 6(a)), which confirms that the actual state is captured by a microcanonical

distribution, eq. (17), as expected. In addition, we can also look at the expectation of the energy to consolidate the analytic estimates. While the grand canonical distribution, eq. (19), describes independent random variables, the microcanonical ensemble, eq. (17), contains non extensive correlations. Nevertheless, we have $\langle c_n \bar{c}_{n-1} \rangle_{mc} = \langle c_n \bar{c}_{n-1} \rangle_{gc} = 0$, because of phase symmetry. Furthermore, eqs. (22) and (23) result in $\langle |c_n|^2 \rangle_{mc} = \langle |c_n|^2 \rangle_{gc} = 1/L$ and $\langle |c_n|^4 \rangle_{mc} = 2/(L(L+1))$ as well as $\langle |c_n|^4 \rangle_{gc} = 2/L^2$, i.e., there are finite size corrections visible when comparing the values of the fourth moment. Hence, the mean value of the energy eq. (2) in the stationary state reads

$$\langle H \rangle_{mc} = 2 - \frac{\alpha}{L+1}, \qquad \langle H \rangle_{gc} = 2 - \frac{\alpha}{L}\,. \tag{24}$$

These two values agree pretty well with the data obtained from direct numerical simulations (see figure 6(b)), while the data do not allow us to decide which of the two values fits better because of the persistent fluctuations in the stationary state. In fact, the size of these fluctuations can be evaluated in terms of the variance of the energy. If we use for simplicity grand canonical expectations, i.e. $\langle |c_n|^{2k} |c_m|^{2\ell} \rangle_{gc} = (k!/L^k)(\ell!/L^\ell)$ for $n \neq m$, we have

$$\langle H^2 \rangle_{gc} - \langle H \rangle_{gc}^2 = \frac{6}{L} - \frac{8\alpha}{L^2} + \frac{5\alpha^2}{L^3}\,. \tag{25}$$

The corresponding standard deviation fits the size of the energy fluctuations in the stationary state perfectly well (see figure 6(b)). In particular, the size of the energy fluctuations does not depend on the noise strength as expected in a microcanonical or grand canonical ensemble. The considerations so far are not able to clarify the dynamics in the stationary state. Time traces of the energy show that correlations increase when the noise amplitude decreases (see figure 6(b)) so that, finally, the deterministic dynamics is restored. The computation of the autocorrelation function of the energy is consistent with a correlation time that scales as $T_{corr} \sim \sigma^{-2}$ (see inset in figure 6(b)), as one would expect from phase diffusion and simple stochastic models like the Kubo oscillator [23].

In summary, the numerical results confirm the expected behaviour that multiplicative noise heats up the system by entropy production. Thanks to the conservation of normalisation, finally, a stationary state emerges, characterised by an infinite temperature.

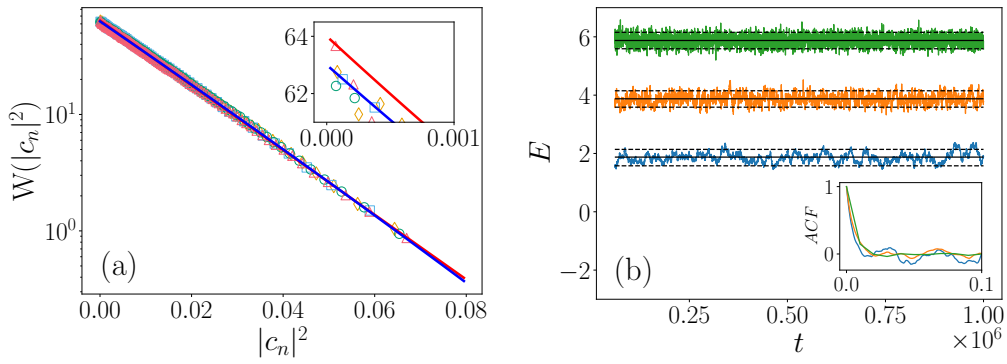

Figure 6: (a) Marginal distribution $W(|c_n|^2) = \pi p(c_n, \bar{c_n})$ in the stationary state for the multiplicative noise model, eq. (14)), for a system of size $L = 64$, $\sigma = 0.1$ and different α values. Symbols: Histogram obtained from about 3.2×10^7 data points of the stationary part of the time series and $\alpha = 2$ (yellow, diamond), $\alpha = 4$ (blue, squares), $\alpha = 6$ (green circles), and $\alpha = 8$ (red triangles). Data are shown on a semi-logarithmic scale. Lines represent the analytic estimates obtained from the microcanonical (orange) and canonical (blue) ensemble, respectively (see eqs. (22) and (23)). The inset shows the data close to zero on a smaller scale. (b) Time traces of the energy, eq. (2), in the stationary state for $\alpha = 8$, a system of size $L = 64$ and different noise levels: $\sigma = 0.01$ (blue), $\sigma = 0.03$ (orange), and $\sigma = 0.1$ (green), cf. Fig. 4(a). The different curves have been displayed with a mutual offset of 2 for visibility. The solid and dashed black horizontal lines indicate the canonical estimate of the mean and the standard deviation of the energy in the stationary state (see eqs. (24) and (25), respectively). The inset shows the corresponding normalised autocorrelation function of the energy on a rescaled time scale $\sigma^2 t$.

3.2. Additive Noise model

As a second example for studying the robustness of breather states against noise, we consider the seemingly simpler case of additive noise, where the equation of motion reads

$$\begin{aligned} \dot{c}_n(t) = i \left(2c_n(t) - c_{n-1}(t) - c_{n+1}(t) - \alpha |c_n(t)|^2 c_n(t)\right) \\ + i\sigma \xi_n(t)\,. \end{aligned} \tag{26}$$

Here, $\xi_n(t)$ denotes again uncorrelated real valued Gaussian noise with correlation given by eq. (15), and the real-valued parameter σ denotes the strength of the noise. This system is, again, a stochastic Hamiltonian system with

Hamiltonian

$$\begin{aligned} H_\sigma(t) &= \sum_{n=0}^{L-1} \Big(2|c_n|^2 - c_n\bar{c}_{n-1} - c_n\bar{c}_{n+1} - \frac{\alpha}{2}|c_n|^4 \\ &\quad +\sigma(c_n + \bar{c}_n)\xi_n(t) \Big) \\ &= H + \sigma \sum_{n=0}^{L-1} (c_n + \bar{c}_n)\xi_n(t)\,. \end{aligned} \tag{27}$$

In this case, normalisation is no longer preserved since $\{H_\sigma(t), N\} \neq 0$, and we expect a completely different dynamical behaviour. For the numerical treatment, we again employ a simple higher-order stochastic symplectic integration scheme (see appendix Appendix A.2 for some details).

Using again the corresponding breather as a localised initial condition, the time traces show an almost linear increase of the normalisation $N(t)$ and an unbounded energy $E(t)$ for a large range of parameter values (see figure 7). In fact, when plotting data on a suitably rescaled time scale, one obtains a reasonable, albeit not perfect, data collapse. One can give a simple heuristic explanation for these numerical findings. While the deterministic part of eq. (26) preserves the normalisation, the additive stochastic force changes N. Hence, we may assume that the stochastic contribution becomes dominant, and the very coarse approximation $\dot{c}_n(t) \sim i\sigma\xi_n(t)$ captures the essence of the phenomena. Hence, the amplitudes c_n obey Brownian motion, and the normalisation follows the average path $N(t) \sim L\sigma^2 t$. This simple reasoning fits the data quite well over a large range of parameter values (see figure 7(b)). If we use the same reasoning to evaluate the energy, eq. (2), we obtain the estimate $E \sim 2L\sigma^2 t - 3L\alpha(\sigma^2 t)^2/2$ so that $\alpha E \sim L(2\alpha\sigma^2 t - 3(\alpha\sigma^2 t)^2/2)$. Again such a simple expression fits the data quite well (see figure 7(a)), even though we do not obtain a perfect data collapse. Hence, to leading order the dynamics of the additive noise model, eq. (26), is dominated by Brownian motion, the amplitudes are unbounded, and no stationary state occurs. In particular, these observations confirm again that the conservation of normalisation is a crucial feature of the DNSE, and any violation of such a conservation law changes the character of the dynamics considerably.

4. Conclusion

We have summarised aspects of localised solutions of the deterministic and stochastic DNSE. Our approach has focused on the impact of the on-site

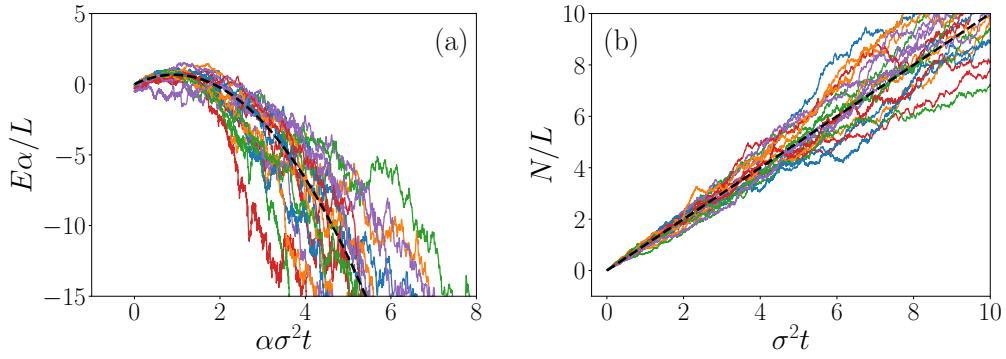

Figure 7: Time traces of (a) the energy scaled by α and of (b) the normalisation obtained from numerical simulations of the additive noise model eq. (27)) with system size $L = 64$ and the breather state (cf. eq. (11)) as an initial condition. Results are shown on a rescaled time scale, $\alpha\sigma^2 t$ and $\sigma^2 t$, respectively. Time traces have been computed for $\alpha = 2$ (blue), $\alpha = 4$ (orange), $\alpha = 6$ (green), $\alpha = 8$ (red), and $\alpha = 10$ (purple) and a range of noise levels $\sigma \in \{0.01, 0.03, 0.1, 0.3\}$. The dashed black lines are the simple analytic estimates $\alpha E/L = 2\alpha\sigma^2 t - 3(\alpha\sigma^2 t)^2/2$ and $N/L = \sigma^2 t$, respectively (see the text for details).

nonlinearity on the dynamics. We constrained the time evolution to states which are normalised to 1. Such a choice is suitable to study systems of finite size but it misses occasionally aspects which become vital in the thermodynamic limit of the model. In that sense our investigations supplement studies of the DNSE which focus on the statistical mechanics of the model.

The investigation of the deterministic DNSE in section 2 essentially coincides with the study of the standardised model, (6), available in the literature. The dynamical features of the localised breather solution of eq. (1), for $\alpha > 0$ (that means the low-temperature behaviour of this model) coincides with the statistical mechanics of eq. (6) when one approaches temperature zero from below (i.e. in the extreme negative temperature regime of the standardised model). Likewise, the low-temperature dynamics of the dynamically conjugate DNSE (1) for $\alpha < 0$ close to the ferromagnetic ground state corresponds to the behaviour of the standardised model (6) when temperature zero is approached from above (i.e. the low-temperature regime of the standardised model). Here the apparent change between ferromagnetic and antiferromagnetic behaviour is contained in the conjugacy between both descriptions. As an aside, one may effectively change the sign of the temperature by changing the sign of the nonlinear term in (1). The stochastic model with multiplicative noise, (14), develops a stationary state which corresponds to the infinite

temperature case of the DNSE. This stochastic model approaches the deterministic case in the limit of small to vanishing noise level in a very peculiar way. While the deterministic DNSE has constant energy, the multiplicative noise model shows a constant variance for the energy which does not depend on the strength of the noise. The stochastic model approaches the deterministic limit by keeping the variance of the energy fixed, but displaying a divergence of the correlation time in the energy autocorrelation function. Hence this peculiar limit is singular. The DNSE with additive noise is a fairly meaningless stochastic model which violates both conservation laws, the conservation of energy and the conservation of normalisation, and thus does not develop any stationary state. This observation emphasises again the importance of nontrivial conserved quantities for the dynamical properties of the DNSE. However, the runaway behaviour of energy and normalization in the model with additive noise can be avoided if one adds suitable dissipation terms. Then, one can set up a stochastic model that naturally leads to a stationary state representing a grandcanonical equilibrium at finite temperature as convincingly demonstrated in [15]. These considerations have been extended recently to cover negative-temperature regimes as well [19].

In our investigation of the DNSE we have used an approach which allows us to switch easily between the positive and the negative temperature regime by changing the sign of the nonlinear term. While the results reported here can be found to some extent in the existing literature in various disguises, we have aimed at a comprehensible account which is accessible for a large audience. We have covered in our exposition two limiting cases, the DNSE for vanishing and for infinite temperature. The more interesting finite temperature cases could be realised by coupling the DNSE to a heat bath. Studying the resulting stochastic model which now includes noise and damping in line with the required dissipation fluctuation relations could give better insight into stationary and dynamical properties of the DNSE, including the negative temperature regime. Our present study prepares the ground for such an investigation.

Acknowledgements

We acknowledge useful discussions with Marco Hofmann during the early stages of this work, who did preliminary investigations of the model during his Master thesis.

Funding and Competing Interests

This work was supported by the German Research Foundation (DFG) under contract number Dr300/16 and via CRC 1270 "Electrically Active Implants", Grant/Award Number SFB 1270/2-299150580.

Appendix A. Symplectic integrators

Numerical integration of Hamiltonian dynamics over large time intervals require integration schemes which preserve the energy, or which preserve a quantity which differs little from the energy, so called symplectic integration schemes. Here, we require integration schemes which preserve in addition the normalisation N. Following the basic ideas of [36], we design second-order schemes for the autonomous and the non-autonomous case.

Appendix A.1. Autonomous system

To design a symplectic integration scheme for eq. (1)) we write the Hamiltonian eq. (2)) as a sum of two parts, $H = H_A + H_B$ with

$$\begin{aligned} H_A &= \sum_{n=0}^{L-1} \left(2|c_n|^2 - c_n\bar{c}_{n-1} - c_n\bar{c}_{n+1}\right) \\ H_B &= -\frac{\alpha}{2}\sum_{n=0}^{L-1} |c_n|^4 \,. \end{aligned} \tag{A.1}$$

Each of these two parts gives rise to a motion that can be computed by analytic means.

If we use $i\mathbf{L}_B|c_n|^2 = \{H_B, |c_n|^2\} = 0$ and $i\mathbf{L}_B c_n = -i\alpha|c_n|^2 c_n$ we obtain for the evolution operator of H_B

$$\exp\left(i\mathbf{L}_B\tau\right) c_n = \exp\left(-i\alpha|c_n|^2\tau\right) c_n \,. \tag{A.2}$$

Likewise, we can handle the dynamics of the Hamiltonian H_A which constitutes the nearest neighbour coupled chain of harmonic oscillators. If we introduce Fourier modes by

$$\hat{c}_q = \sum_{n=0}^{L-1} \exp(iqn) c_n, \quad q = 2\pi\nu/L, \quad \nu = 0, 1, \ldots, L-1 \tag{A.3}$$

we have

$$
\begin{aligned}
i\mathbf{L}_A\hat{c}_q &= i\sum_{n=0}^{L-1}\exp(iqn)\left(2c_n - c_{n-1} - c_{n+1}\right) \\
&= i2(1-\cos(q))\hat{c}_q
\end{aligned}
\tag{A.4}
$$

so that

$$
\exp\left(i\mathbf{L}_A\tau\right)\hat{c}_q = \exp\left(i2(1-\cos(q))\tau\right)\hat{c}_q\,. \tag{A.5}
$$

Thus using the Fourier transform eq. (A.3)) and its inverse the evolution operator of H_A can be written in closed form

$$
\begin{aligned}
\exp\left(i\mathbf{L}_A\tau\right)c_n = \frac{1}{L}\sum_q \exp(-iqn)\exp\left(i2(1-\cos(q))\tau\right) \\
\sum_{m=0}^{L-1}\exp\left(imq\right)c_m\,.
\end{aligned}
\tag{A.6}
$$

To evaluate the sums in eq. (A.6)) efficiently, one first computes the Fourier transform of the state $\{c_n\}$ (see eq. (A.3))), evaluates then the time evolution of each Fourier mode by eq. (A.5)), and finally performs an inverse Fourier transform.

If τ denotes the stepsize of a numerical integration scheme, we can approximate the exact evolution operator of eq. (1)), $\exp(i(\mathbf{L}_A+\mathbf{L}_B)\tau)$, up to second order by

$$
\begin{aligned}
\exp\left(i(\mathbf{L}_A+\mathbf{L}_B)\tau\right) = &\exp\left(i\mathbf{L}_B\tau/2\right)\exp\left(i\mathbf{L}_A\tau\right) \\
&\exp\left(i\mathbf{L}_B\tau/2\right) + \mathcal{O}(\tau^3)
\end{aligned}
\tag{A.7}
$$

as can be straightforwardly verified by using the series expansion of the exponentials. The right-hand side provides a symplectic integration scheme with a one-step error of order $\mathcal{O}(\tau^3)$ since each of the three factors can be evaluated up to machine precision. (i) One first applies eq. (A.2)) to a state $\{c_n\}$ with time step $\tau/2$ to obtain an intermediate result. (ii) One then applies eq. (A.6)) to this intermediate result, using a Fourier transform, eq. (A.5)), and an inverse Fourier transform. (iii) Finally one applies eq. (A.2)) again with time $\tau/2$ to obtain the final state $\{c_n\}$ of this symplectic integration step. By design, the scheme preserves an energy which differs from eq. (2)) by an amount of order $\mathcal{O}(\tau^2)$ (see figure 3(b)). In addition, the normalisation is preserved to machine precision (see figure 3(c)), since $i\mathbf{L}_A N = 0$ and $i\mathbf{L}_B N = 0$.

Appendix A.2. Stochastic systems

To design a symplectic integration step for stochastic systems, let us first consider the case of a non-autonomous Hamiltonian system, where the Hamiltonian can be split into two parts, $H(t) = H_A + H_B(t)$, and where we assume for simplicity that $\{H_B(t), H_B(t')\} = 0$. The evolution operator of the non-autonomous system obeys

$$\frac{\partial \mathbf{U}(t_0,t)}{\partial t} = \mathbf{U}(t_0,t) i\mathbf{L}(t), \quad \mathbf{U}(t_0,t_0) = \mathbf{1}\,. \tag{A.8}$$

The Neumann series up to terms of second order can be easily obtained by iteration

$$\begin{aligned}
\mathbf{U}(t_0,t_0+\tau) &= \mathbf{1} + \int_{t_0}^{t_0+\tau} \mathbf{U}(t_0,t) i\mathbf{L}(t) dt \\
&= \mathbf{1} + i\mathbf{L}_A\tau + i\int_{t_0}^{t_0+\tau} \mathbf{L}_B(t) dt \\
&\quad + \int_{t_0}^{t_0+\tau}\int_{t_0}^{t} (i\mathbf{L}_A + i\mathbf{L}_B(s)) \\
&\quad (i\mathbf{L}_A + i\mathbf{L}_B(t))\, ds dt + \mathcal{O}(\tau^3) \\
&= \mathbf{1} + i\mathbf{L}_A\tau + (i\mathbf{L}_B^< + i\mathbf{L}_B^>)\,\tau \\
&\quad + (i\mathbf{L}_A)^2 \frac{\tau^2}{2} + i\mathbf{L}_A i\mathbf{L}_B^> \tau^2 + i\mathbf{L}_B^< i\mathbf{L}_A \tau^2 \\
&\quad + (i\mathbf{L}_B^< + i\mathbf{L}_B^>)^2 \frac{\tau^2}{2} + \mathcal{O}(\tau^3)
\end{aligned} \tag{A.9}$$

where we have introduced the abbreviations

$$\begin{aligned}
i\mathbf{L}_B^< &= \tau^{-2}\int_{t_0}^{t_0+\tau}\int_{t_0}^{t} i\mathbf{L}_B(s) ds dt \\
&= \tau^{-2}\int_{t_0}^{t_0+\tau} (t_0+\tau-s) i\mathbf{L}_B(s) ds \\
i\mathbf{L}_B^> &= \tau^{-2}\int_{t_0}^{t_0+\tau}\int_{t_0}^{t} i\mathbf{L}_B(t) ds dt \\
&= \tau^{-2}\int_{t_0}^{t_0+\tau} (t-t_0) i\mathbf{L}_B(t) dt\,.
\end{aligned} \tag{A.10}$$

eq. (A.9)) can be written as a product of suitable exponentials, namely (cf. eq. (A.7)))

$$\begin{aligned}\mathbf{U}(t_0, t_0+\tau) = &\exp\left(i\mathbf{L}_B^{\leqslant}\tau\right)\exp\left(i\mathbf{L}_A\tau\right)\exp\left(i\mathbf{L}_B^{>}\tau\right)\\ &+\mathcal{O}(\tau^3)\,.\end{aligned} \tag{A.11}$$

We will base our symplectic integration step on such an identity. This means that we are implementing noise in the sense of Stratonovich, who treats the stochastic term as the limit of a continuous function.

i): For the SDNSE with multiplicative noise, eq. (14)), we use

$$\begin{aligned} H_A &= \sum_{n=0}^{L-1}\left(2|c_n|^2 - c_n\bar{c}_{n-1} - c_n\bar{c}_{n+1}\right)\\ H_B(t) &= \sum_{n=0}^{L-1}\left(-\frac{\alpha}{2}|c_n|^4 + \sigma|c_n|^2\xi_n(t)\right)\end{aligned} \tag{A.12}$$

to write the Hamiltonian eq. (16)) as a sum of two parts $H(t) = H_A + H_B(t)$. Obviously the time-dependent part obeys $\{H_B(t), H_B(t')\} = 0$. Eq. (A.10)) yields for the effective Hamiltonians $H_B^{\leqslant}$ and $H_B^{>}$

$$H_B^{\leqslant} = \frac{1}{2}\sum_{n=0}^{L-1}\left(-\frac{\alpha}{2}\right)|c_n|^4 + \sum_{n=0}^{L-1}\sigma|c_n|^2\frac{D_n^{\leqslant}}{\sqrt{\tau}} \tag{A.13}$$

where we have introduced the Gaussian random variables $D_n^{\leqslant}$ by

$$\begin{aligned} D_n^{<} &= \tau^{-3/2}\int_{t_0}^{t_0+\tau}(t_0+\tau-t)\xi_n(t)dt\\ D_n^{>} &= \tau^{-3/2}\int_{t_0}^{t_0+\tau}(t-t_0)\xi_n(t)dt\,.\end{aligned} \tag{A.14}$$

For the correlations of these random variables, we obtain with the help of eq. (15))

$$\begin{aligned}
\langle D_n^< D_m^< \rangle &= \delta_{n,m}\tau^{-3}\int_{t_0}^{t_0+\tau}(t_0+\tau-t)^2 dt = \frac{1}{3}\delta_{n,m} \\
\langle D_n^> D_m^> \rangle &= \delta_{n,m}\tau^{-3}\int_{t_0}^{t_0+\tau}(t-t_0)^2 dt = \frac{1}{3}\delta_{n,m} \\
\langle D_n^< D_m^> \rangle &= \delta_{n,m}\tau^{-3}\int_{t_0}^{t_0+\tau}(t_0+\tau-t)(t-t_0) dt \\
&= \frac{1}{6}\delta_{n,m}\,. \qquad \text{(A.15)}
\end{aligned}$$

eq. (A.13)) results in $i\mathbf{L}_B^{\lessgtr}|c_n|^2 = 0$ and $i\mathbf{L}_B^{\lessgtr} = -i\alpha|c_n|^2 c_n/2 + i\sigma D_n^{\lessgtr}/\sqrt{\tau}$ so that (cf. eq. (A.2)))

$$\exp\left(i\mathbf{L}_B^{\lessgtr}\tau\right) c_n = \exp\left(-i\alpha|c_n|^2\tau/2 + i\sigma D_n^{\lessgtr}\sqrt{\tau}\right) c_n\,. \qquad \text{(A.16)}$$

For the action of $\exp(i\mathbf{L}_A\tau)$ we can simply refer to the previous section Appendix A.1, eqs.(A.3)-(A.6).

We now apply eq. (A.11)) to generate a symplectic integration step for the SDNSE, eq. (14)), keeping in mind that the stochastic one-step error is of order $\mathcal{O}(\tau^2)$ due to the lack of smoothness of random functions. Given a state $\{c_n\}$ one generates correlated random numbers $D_n^{\lessgtr}$ from suitable linear combinations of uncorrelated normal random variables. (i) First[1] one applies eq. (A.16)) with random variables $D_n^<$ to generate an intermediate state. (ii) Then one performs a Fourier transform, applies eq. (A.5)), and performs an inverse Fourier transform. (iii) Finally, we use again eq. (A.16)) with random variables $D_n^>$ to obtain the final state of the numerical integration scheme. Since $i\mathbf{L}_A N = 0$ and $i\mathbf{L}_B^{\lessgtr} N = 0$ the numerical scheme preserves the normalisation.

[1]Recall that $\exp\big(i\mathbf{L}_{a/b}\tau\big)c = F_{a/b}(c)$ implies $\exp(i\mathbf{L}_a\tau)\exp(\mathbf{L}_b\tau)c = \exp(i\mathbf{L}_a\tau)F_b(c) = F_b(F_a(c))$.

ii): For the SDNSE with additive noise, eq. (17)), we use

$$\begin{aligned} H_A &= \sum_{n=0}^{L-1} \left(2|c_n|^2 - c_n \bar{c}_{n-1} - c_n \bar{c}_{n+1} - \frac{\alpha}{2} |c_n|^4 \right) \\ H_B(t) &= \sigma \sum_{n=0}^{L-1} (c_n + \bar{c}_n)\, \xi_n(t) \end{aligned} \tag{A.17}$$

to write the Hamiltonian eq. (18)) as a sum of two parts $H(t) = H_A + H_B(t)$. Obviously the time-dependent part obeys $\{H_B(t), H_B(t')\} = 0$. Eq. (A.10)) yields for the effective Hamiltonians $H_B^<$ and $H_B^>$

$$H_B^{\lessgtr} = \sigma \sum_{n=0}^{L-1} (c_n + \bar{c}_n)\, \frac{D_n^{\lessgtr}}{\sqrt{\tau}} \tag{A.18}$$

where $D_n^{\lessgtr}$ again denote the random variables defined in eq. (A.14)) and (A.15). Since $i\mathbf{L}_B^{\lessgtr} c_n = i\sigma D_n^{\lessgtr}/\sqrt{\tau}$ we have (cf. eq. (A.16)))

$$\exp\left(i\mathbf{L}_B^{\lessgtr}\tau\right) c_n = c_n + i\sigma D_n^{\lessgtr} \sqrt{\tau}\,. \tag{A.19}$$

Since H_A in eq. (A.17)) coincides with the Hamiltonian of the DNSE, eq. (2)) we can evaluate $\exp(i\mathbf{L}_A\tau)$ (up to and including second order terms) by the scheme described in section Appendix A.1, cf. eq. (A.7)).

We now use again eq. (A.11)) to design a symplectic integration step with one-step error of order $\mathcal{O}(\tau^2)$. Given a state $\{c_n\}$ one generates correlated random numbers $D_n^{\lessgtr}$ from suitable linear combinations of uncorrelated normal random variables. (i) The first one applies eq. (A.19)) with random variables $D_n^<$ to generate an intermediate state. (ii) Then, following the steps of section Appendix A.1 one applies eq. (A.2)) with time step $\tau/2$ to the intermediate state, performs a Fourier transform, applies eq. (A.5)) to the Fourier components, performs an inverse Fourier transform, and applies eq. (A.2)) again with time $\tau/2$. (iii) Finally we use eq. (A.19)) with random variables $D_n^>$ to obtain the result of the symplectic integration step.

References

[1] Baldovin, M., Iubini, S., Livi, R., Vulpiani, A., 2021. Statistical mechanics of systems with negative temperature. Physics Reports 923, 1–50. doi:10.1016/j.physrep.2021.03.007.

[2] de Bouard, A., Debussche, A., 1999. A Stochastic Nonlinear Schrödinger Equation with Multiplicative Noise. Communications in Mathematical Physics 205, 161–181. URL: https://doi.org/10.1007/s002200050672, doi:10.1007/s002200050672.

[3] Carlen, E.A., Fröhlich, J., Lebowitz, J., 2016. Exponential Relaxation to Equilibrium for a One-Dimensional Focusing Non-Linear Schrödinger Equation with Noise. Communications in Mathematical Physics 342, 303–332. URL: https://doi.org/10.1007/s00220-015-2511-9, doi:10.1007/s00220-015-2511-9.

[4] Carlen, E.A., Fröhlich, J., Lebowitz, J., Wang, W.M., 2019. Quantitative bounds on the rate of approach to equilibrium for some one-dimensional stochastic nonlinear schrödinger equations. Nonlinearity 32, 1352. URL: https://dx.doi.org/10.1088/1361-6544/aae69c, doi:10.1088/1361-6544/aae69c.

[5] Chatterjee, S., 2014. Invariant Measures and the Soliton Resolution Conjecture. Communications on Pure and Applied Mathematics 67, 1737–1842. URL: https://onlinelibrary.wiley.com/doi/abs/10.1002/cpa.21501, doi:10.1002/cpa.21501.

[6] Chatterjee, S., Kirkpatrick, K., 2012. Probabilistic Methods for Discrete Nonlinear Schrödinger Equations. Communications on Pure and Applied Mathematics 65, 727–757. URL: https://onlinelibrary.wiley.com/doi/abs/10.1002/cpa.21388, doi:10.1002/cpa.21388.

[7] Eilbeck, J., Johansson, M., 2003. The discrete nonlinear Schrödinger equation - 20 years on, in: Vázquez, R., MacKay, R., Zorzano, M. (Eds.), Localization and Energy transfer in Nonlinear Systems. World Scientific, Singapore, p. 44.

[8] Flach, S., Willis, C., 1998. Discrete breathers. Phys. Rep. 295, 181. doi:https://doi.org/10.1016/S0370-1573(97)00068-9.

[9] Franzosi, R., Livi, R., Oppo, G.L., Politi, A., 2011. Discrete breathers in bose–einstein condensates. Nonlinearity 24, R89. URL: https://dx.doi.org/10.1088/0951-7715/24/12/R01, doi:10.1088/0951-7715/24/12/R01.

[10] Hairer, E., Lubich, C., Wanner, G., 2006. Geometric Numerical Integration. Structure-Preserving Algorithms for Ordinary Differential Equations. volume 31 of *Springer Series in Computational Mathematics*. Springer, New York. doi:10.1007/3-540-30666-8.

[11] Hannani, A., Olla, S., 2023. A stochastic thermalization of the Discrete Nonlinear Schrödinger Equation. Stochastics and Partial Differential Equations: Analysis and Computations 11, 1379–1415. URL: https://doi.org/10.1007/s40072-022-00263-9, doi:10.1007/s40072-022-00263-9.

[12] Hennig, D., Tsironis, G., 1999. Wave transmission in nonlinear lattices. Physics Reports 307, 333–432. URL: https://www.sciencedirect.com/science/article/pii/S0370157398000258, doi:https://doi.org/10.1016/S0370-1573(98)00025-8.

[13] Holstein, T., 1959. Studies of polaron motion: Part i. the molecular-crystal model. Annals of Physics 8, 325–342. URL: https://www.sciencedirect.com/science/article/pii/0003491659900028, doi:https://doi.org/10.1016/0003-4916(59)90002-8.

[14] Iubini, S., Chirondojan, L., Oppo, G.L., Politi, A., Politi, P., 2019. Dynamical freezing of relaxation to equilibrium. Phys. Rev. Lett. 122, 084102. URL: https://link.aps.org/doi/10.1103/PhysRevLett.122.084102, doi:10.1103/PhysRevLett.122.084102.

[15] Iubini, S., Lepri, S., Livi, R., Politi, A., 2013. Off-equilibrium Langevin dynamics of the discrete nonlinear Schrödinger chain. J. Stat. Mech 2013, P08017. URL: https://iopscience.iop.org/article/10.1088/1742-5468/2013/08/P08017, doi:10.1088/1742-5468/2013/08/P08017.

[16] Iubini, S., Franzosi, R., Livi, R., Oppo, G.L., Politi, A., 2013. Discrete breathers and negative-temperature states. New Journal of Physics 15, 023032. URL: https://dx.doi.org/10.1088/1367-2630/15/2/023032, doi:10.1088/1367-2630/15/2/023032.

[17] Iubini, S., Politi, A., Politi, P., 2014. Coarsening Dynamics in a Simplified DNLS Model. Journal of Statistical Physics 154, 1057–1073.

URL: https://doi.org/10.1007/s10955-013-0896-4, doi:10.1007/s10955-013-0896-4.

[18] Iubini, S., Politi, A., Politi, P., 2017. Relaxation and coarsening of weakly-interacting breathers in a simplified DNLS chain. J. Stat. Mech. 73, 073201. URL: https://doi.org/10.1088/1742-5468/aa7871, doi:10.1088/1742-5468/aa7871.

[19] Iubini, S., Politi, A., 2025. Effective grand canonical description of condensation in negative-temperature regimes. Phys. Rev. Lett. 134, 097102. URL: https://doi.org/10.1103/PhysRevLett.134.097102, doi:10.1103/PhysRevLett.134.097102.

[20] Johansson, M., Aubry, S., 1997. Existence and stability of quasiperiodic breathers in the discrete nonlinear schrödinger equation. Nonlinearity 10, 1151–1178. URL: https://iopscience.iop.org/article/10.1088/0951-7715/10/5/008, doi:10.1088/0951-7715/10/5/008.

[21] Johansson, M., Rasmussen, K.Ø., 2004. Statistical mechanics of general discrete nonlinear schrödinger models: Localization transition and its relevance for klein-gordon lattices. Phys. Rev. E 70, 066610. URL: https://link.aps.org/doi/10.1103/PhysRevE.70.066610, doi:10.1103/PhysRevE.70.066610.

[22] Kevrekidis, P.G., 2009. The Discrete Nonlinear Schrödinger Equation: Mathematical Analysis, Numerical Computations and Physical Perspectives. volume 232 of *Springer Tracts in Modern Physics*. Springer, Berlin, Heidelberg. URL: https://link.springer.com/10.1007/978-3-540-89199-4, doi:10.1007/978-3-540-89199-4.

[23] Kubo, R., 1962. A stochastic theory of line shape and relaxation, in: ter Haar, D. (Ed.), Fluctuation, relaxation, and resonance in magnetic systems. Oliver and Boyd, Edinburgh, pp. 23–66.

[24] Pfirsch, D., 1990. Nonlinear instabilities, negative energy modes and generalized cherry oscillators. Z. Naturforsch. A 45, 839. doi:https://doi.org/10.1515/zna-1990-0701.

[25] Rasmussen, K., Aubry, S., Bishop, A., Tsironis, G., 2000a. Discrete nonlinear Schrödinger breathers in a phonon bath. The European Physical

Journal B - Condensed Matter and Complex Systems 15, 169–175. URL: https://doi.org/10.1007/PL00011032, doi:10.1007/PL00011032.

[26] Rasmussen, K.Ø., Cretegny, T., Kevrekidis, P.G., Grønbech-Jensen, N., 2000b. Statistical Mechanics of a Discrete Nonlinear System. Physical Review Letters 84, 3740–3743. URL: https://link.aps.org/doi/10.1103/PhysRevLett.84.3740, doi:10.1103/PhysRevLett.84.3740.

[27] Rumpf, B., 2004. Simple statistical explanation for the localization of energy in nonlinear lattices with two conserved quantities. Physical Review E 69, 016618. URL: https://link.aps.org/doi/10.1103/PhysRevE.69.016618, doi:10.1103/PhysRevE.69.016618.

[28] Rumpf, B., 2007. Growth and erosion of a discrete breather interacting with rayleigh-jeans distributed phonons. Europhysics Letters 78, 26001. URL: https://dx.doi.org/10.1209/0295-5075/78/26001, doi:10.1209/0295-5075/78/26001.

[29] Rumpf, B., 2008. Transition behavior of the discrete nonlinear Schrödinger equation. Physical Review E 77, 036606. URL: https://link.aps.org/doi/10.1103/PhysRevE.77.036606, doi:10.1103/PhysRevE.77.036606.

[30] Rumpf, B., 2009. Stable and metastable states and the formation and destruction of breathers in the discrete nonlinear schrödinger equation. Physica D: Nonlinear Phenomena 238, 2067–2077. URL: https://www.sciencedirect.com/science/article/pii/S0167278909002541, doi:https://doi.org/10.1016/j.physd.2009.08.006.

[31] Rumpf, B., Newell, A., 2001. Coherent structures and entropy in constrained, modulationally unstable, nonintegrable systems. Phys. Rev. Lett. 87, 054102. doi:https://doi.org/10.1103/PhysRevLett.87.054102.

[32] Scott, A., 2003. Nonlinear Science: Emergence and Dynamics of Coherent Structures. Oxford University Press. URL: https://doi.org/10.1093/oso/9780198528524.001.0001, doi:10.1093/oso/9780198528524.001.0001.

[33] Skokos, C., Gerlach, E., Bodyfelt, J., Papamikos, G., Eggl, S., 2014. High order three part split symplectic integrators: Efficient techniques for the long time simulation of the disordered discrete nonlinear Schrödinger equation. Physics Letters A 378, 1809–1815. doi:10.1016/j.physleta.2014.04.050.

[34] Szavits-Nossan, J., Evans, M., Majumdar, S.N, 2014. Constraint-driven condensation in large fluctuations of linear statistics. Phys. Rev. Lett. 112, 020602. URL: https://link.aps.org/doi/10.1103/PhysRevLett.112.020602, doi:10.1103/PhysRevLett.112.020602.

[35] Trombettoni, A., Smerzi, A., 2001. Discrete solitons and breathers with dilute bose-einstein condensates. Phys. Rev. Lett. 86, 2353–2356. URL: https://link.aps.org/doi/10.1103/PhysRevLett.86.2353, doi:10.1103/PhysRevLett.86.2353.

[36] Yoshida, H., 1990. Construction of higher order symplectic integrators. Phys.Lett. A 150, 262. doi:https://doi.org/10.1016/0375-9601(90)90092-3.